Neurobiology of Disease 124 (2019) 428–438

Contents lists available at ScienceDirect

Neurobiology of Disease

journal homepage: www.elsevier.com/locate/ynbdi

Decreased circulating ErbB4 ectodomain fragments as a read-out of impaired signaling function in amyotrophic lateral sclerosis

Inmaculada Lopez-Font[a,b,1], Aitana Sogorb-Esteve[a,b,1], Míriam Javier-Torrent[b,c], Gunnar Brinkmalm[d,e], Mireia Herrando-Grabulosa[b,f], Belen García-Lareu[b,c], Janina Turon-Sans[g,h], Ricardo Rojas-García[g,h], Alberto Lleó[b,i], Carlos A. Saura[b,c], Henrik Zetterberg[d,e,j,k], Kaj Blennow[d,e], Assumpció Bosch[b,c], Xavier Navarro[b,f], Javier Sáez-Valero[a,b,*]

[a] Instituto de Neurociencias de Alicante, Universidad Miguel Hernández-CSIC, Sant Joan d'Alacant, Spain
[b] Centro de Investigación Biomédica en Red sobre Enfermedades Neurodegenerativas (CIBERNED), Spain
[c] Institut de Neurociències, Department of Biochemistry and Molecular Biology, Universitat Autònoma de Barcelona, Bellaterra, Spain
[d] Clinical Neurochemistry Laboratory, Sahlgrenska University Hospital, Mölndal, Sweden
[e] Institute of Neuroscience and Physiology, University of Gothenburg, Mölndal, Sweden
[f] Institut de Neurociències and Department of Cell Biology, Physiology and Immunology, Universitat Autònoma de Barcelona, Bellaterra, Spain
[g] Neuromuscular Diseases Unit, Department of Neurology, Hospital de la Santa Creu i Sant Pau, Universitat Autònoma de Barcelona, Barcelona, Spain
[h] Centro de Investigación Biomédica en Red de Enfermedades Raras (CIBERER), Spain
[i] Memory Unit, Neurology Department, Hospital de la Santa Creu i Sant Pau, Barcelona, Spain
[j] Department of Neurodegenerative Disease, Institute of Neurology, University College London, London, UK
[k] UK Dementia Research Institute at UCL, London, UK

ARTICLE INFO

Keywords:
Amyotrophic lateral sclerosis
ErbB4
Biomarker
Cerebrospinal fluid
Brain
Plasma
ALS transgenic mouse

ABSTRACT

ErbB4 is a transmembrane receptor tyrosine kinase that binds to neuregulins to activate signaling. Proteolytic cleavage of ErbB4 results in release of soluble fragments of ErbB4 into the interstitial fluid. Disruption of the neuregulin-ErbB4 pathway has been suggested to be involved in the pathogenesis of amyotrophic lateral sclerosis (ALS). This study assesses whether soluble proteolytic fragments of the ErbB4 ectodomain (ecto-ErbB4) can be detected in cerebrospinal fluid (CSF) and plasma, and if the levels are altered in ALS. Immunoprecipitation combined with mass spectrometry or western blotting analyses confirmed the presence of ecto-ErbB4 in human CSF. Several anti-ErbB4-reactive bands, including a 55 kDa fragment, were detected in CSF. The bands were generated in the presence of neuregulin-1 (Nrg1) and were absent in plasma from ErbB4 knockout mice. Ecto-ErbB4 levels were decreased in CSF from ALS patients (n = 20) and ALS with concomitant frontotemporal dementia patients (n = 10), compared to age-matched controls (n = 13). A similar decrease was found for the short ecto-ErbB4 fragments in plasma of the same subjects. Likewise, the 55-kDa ecto-ErbB4 fragments were decreased in the plasma of the two transgenic mouse models of ALS ($SOD1^{G93A}$ and $TDP\text{-}43^{A315T}$). Intracellular ErbB4 fragments were decreased in the frontal cortex from $SOD1^{G93A}$ mice, indicating a reduction in Nrg-dependent induction of ErbB4 proteolytic processing, and suggesting impaired signaling. Accordingly, overexpression of Nrg1 induced by an adeno-associated viral vector increased the levels of the ecto-ErbB4 fragment in the $SOD1^{G93A}$ mice. We conclude that the determination of circulating ecto-ErbB4 fragments could be a tool to evaluate the impairment of the ErbB4 pathway and may be a useful biomarker in ALS.

Abbreviations: ErbB4, Erb-B2 Receptor Tyrosine Kinase 4; ecto-ErbB4, ErbB4 ectodomain; ErbB4-CTF, ErbB4 C-terminal fragment; ErbB4-ICD, ErbB4 intracellular domain; ALS, amyotrophic lateral sclerosis; FTD, frontotemporal dementia; ALS-FTD, ALS with concomitant frontotemporal dementia; CSF, cerebrospinal fluid; Nrg1, neuregulin-1; AAV, adeno-associated viral

* Corresponding author at: Instituto de Neurociencias de Alicante, Universidad Miguel Hernández-CSIC, Av. Ramón y Cajal s/n, 03550 Sant Joan d'Alacant, Spain.
E-mail address: j.saez@umh.es (J. Sáez-Valero).

[1] I. Lopez-Font and A. Sogorb-Esteve contributed equally to this study.

https://doi.org/10.1016/j.nbd.2018.12.021
Received 24 July 2018; Received in revised form 6 December 2018; Accepted 26 December 2018
Available online 27 December 2018
0969-9961/

1. Introduction

ErbB4 (Erb-B2 Receptor Tyrosine Kinase 4) is a single-pass type I transmembrane receptor that contains a cytoplasmic tyrosine kinase domain (Plowman et al., 1993). ErbB4 is a member of the epidermal growth factor (EGF) receptor subfamily that binds and is activated by neuregulins (Nrg1, Nrg2, Nrg3 and Nrg4), heparin-binding EGF-like growth factor and other members of the EGF family such as betacellulin. Ligand binding triggers ErbB receptor dimerization and autophosphorylation at specific tyrosine residues, after which activated ErbB receptors serve as binding sites for scaffold proteins and effectors, transducing cellular responses. ErbB4 induces a variety of cellular responses including cell proliferation and differentiation (reviewed in Carpenter, 2003 and in Roskoski, 2014).

Amyotrophic lateral sclerosis (ALS) is a neurological disease characterized by the degeneration of upper and lower motor neurons that causes inexorable progressive muscle weakness. Patients with ALS may also exhibit a wide range of cognitive and behavioral abnormalities and as many as 20% show signs that fulfill criteria for frontotemporal dementia (FTD) mainly in its behavioral variant (Lomen-Hoerth et al., 2003; Phukan et al., 2012; Ringholz et al., 2005). There is also pathological and molecular evidence of an overlap between ALS and FTD, suggesting that these diseases represent different manifestations of a similar spectrum (Lillo and Hodges, 2010).

Mutations in the *ERBB4* gene support a role for the ErbB4 protein in ALS (Takahashi et al., 2013). Possible pathogenic mutations in the *ERBB4* gene have been also recently described in concomitant ALS and FTD (Dols-Icardo et al., 2018). These mutations on the *ERBB4* gene appear to be loss-of-function mutations, since they cause amino acid substitutions within the tyrosine kinase domain, which lead to reduced autophosphorylation of ErbB4 upon Nrg1 stimulation (Takahashi et al., 2013). A decrease in the amount of Nrg1-III isoforms has been detected in the spinal motor neurons in familiar and sporadic ALS individuals and in ALS mutant mice at disease onset (Song et al., 2012). All these reports raise the possibility that disruption of the Nrg1/ErbB4 pathway is involved in the pathogenesis of ALS.

Nrg1-binding not only induces activation of ErbB4, but also the ensuing sequential proteolytic cleavage of the receptor (Sardi et al., 2006), firstly by the metalloprotease ADAM17 (TNF-α-converting enzyme; TACE), which causes the secretion of an N-terminal ecto-domain fragment (ecto-ErbB4) (Rio et al., 2000). The remaining C-terminal fragment (ErbB4-CTF) is processed by γ-secretase/presenilin1 (PS1), generating shorter intracellular domain (ErbB4-ICD) fragments (Ni et al., 2001). This ErbB4-ICD fragment can translocate to the nucleus retaining tyrosine kinase activity (Bao et al., 2003; Vecchi and Carpenter, 1997), and can regulate gene expression (Ancot et al., 2009; Sardi et al., 2006). Other metalloproteases, identified in various cell types, can also promote ectodomain cleavage of several ErbB receptors including ErbB4 (Lynch et al., 2007; Sanderson et al., 2006; Yu et al., 2002). The soluble extracellular ecto-ErbB4 fragments resulting from metalloprotease cleavage also exhibit biological activity, binding Nrg1 and blocking autocrine and paracrine signaling (Ma et al., 2009; Tian et al., 2017; Wen et al., 2010; Woo et al., 2007). Thus, ecto-ErbB4 has been suggested to influence brain activity, to regulate synaptic plasticity (Chen et al., 2010), anxiety-like behavior (Geng et al., 2016), and furthermore exhibits potential as a drug target candidate (Gambarotta et al., 2015; Pascal et al., 2014).

The soluble ecto-ErbB4 fragments are expected to be present in circulatory fluids (Baron et al., 2009). Indeed, ecto-ErbB4 fragments have been detected in the medium of cultured cancer cells (Hollmén et al., 2012, 2009). However, to our knowledge, circulating ecto-ErbB4 levels have not yet been assessed in CSF and/or plasma of patients suffering neurodegenerative disorders.

In this study, we investigated if truncated soluble ecto-ErbB4 is detectable in CSF and plasma of ALS and ALS-FTD patients and in plasma of transgenic ALS mouse models. We characterized a 55-kDa ecto-ErbB4 fragment in plasma and CSF and we found it to be reduced in ALS patients. Additionally, this 55-kDa ecto-ErbB4 fragment increased in parallel with Nrg1 expression. Moreover, in the brain of ALS transgenic mice, we also observed impairment in the ErbB4 proteolytic processing rate, indicative of failure in this signaling pathway.

2. Materials and methods

2.1. Patients, CSF and plasma samples

This study was approved by the local ethics committees of all the centers involved and it was carried out in accordance with the Helsinki Declaration. CSF and plasma samples from patients with ALS were obtained from the Motor Neuron Disease Clinic and the Memory Unit at the Hospital de la Santa Creu i Sant Pau, Barcelona, Spain. Patients included in the study fulfilled *El Escorial* revised criteria for probable, probable laboratory-supported or definite ALS (Brooks et al., 2000). All of the patients underwent cognitive and behavioral screening and were classified as ALS without cognitive or behavioral impairment or ALS-FTD according to the criteria described by Strong et al. (2017). Participants included 30 ALS patients (18 men and 12 women, 67 ± 2 years), 20 of them without cognitive and behavioral abnormalities (12 men and 8 women, 65 ± 2 years) and 10 ALS cases with concomitant FTD (ALS-FTD; 6 men and 4 women, 72 ± 2 years) (Illlán-Gala et al., 2018). The mean age at the appearance of the motor symptoms was 65 ± 2 years, with a mean time delay from onset to lumbar puncture of 30.2 ± 5.2 months. Seven cases were bulbar (23%), twenty-two cases (73%) were spinal onset, and one case was respiratory onset. All the ALS patients received riluzole. Thirteen ALS patients had died by the end of the study (average survival time 40.1 ± 7.1 months).

Age-matched cognitively normal controls were randomly selected from the Sant Pau Initiative on Neurodegeneration (SPIN cohort: https://santpaumemoryunit.com/our-research/spin-cohort/) (Alcolea et al., 2017). Controls had no history, symptoms or signs of neurological or psychiatric disorders, or memory complaints (n = 13; 9 men and 4 women, 68 ± 1 years) and had normal levels of core Alzheimer's disease biomarkers in CSF (Alcolea et al., 2015).

Plasma samples were from the same individuals, except for one ALS subject that lacked a plasma sample (n = 29; 17 men and 12 women, 67 ± 2 years). Samples were collected in heparinized tubes and separated from whole blood by centrifugation at 3000 × g for 15 min at 4 °C. CSF and plasma samples were aliquoted and frozen at −80 °C pending analysis.

2.2. ALS animal models and ErbB4 knock-out mice, plasma samples

Animal care and experimental procedures were approved by the Biosafety and the Ethical Committees of the Universitat Autònoma de Barcelona. Plasma samples were collected from ten 12-week-old (G93A) superoxide dismutase 1 (SOD1) mice (B6SJL-Tg[SOD1-G93A]1Gur; obtained from the Jackson Laboratory), the most widely used ALS mouse model, and ten wild-type littermates. The $SOD1^{G93A}$ transgenic mice recapitulate the most relevant clinical and histopathological features of both familial and sporadic ALS, developing rapidly progressive motoneuron loss, with locomotor deficits from 12 to 13 weeks of age, hindlimb weakness and muscle atrophy, culminating in paralysis and death between ages 16 and 19 weeks (Mancuso et al., 2011; Ripps et al., 1995). For some experiments, plasma samples were also collected from TAR-DNA binding protein-43 (TDP-43) mutant (A315T) mice and littermates (originally from the Jackson Laboratory; generous gift of J. Fernandez-Ruiz, Department of Biochemistry and Molecular Biology, Faculty of Medicine, Complutense University, Madrid, Spain). $TDP\text{-}43^{A315T}$ mice are an alternative ALS transgenic model which also present with features of FTD (Wegorzewska et al., 2009). The plasma samples from the $TDP\text{-}43^{A315T}$ transgenic mice were also collected from

12-week-old animals, since this age represents an early symptomatic stage (Wegorzewska et al., 2009).

Plasma samples were also collected from P50 ErbB4 knockout mice and from littermates controls (ErbB4-KO, kindly provided by B. Rico, Institute of Psychiatry, Psychology and Neuroscience, King's College London, London, UK; see Tidcombe et al., 2003).

Plasma samples were obtained from mice following anesthesia by isofluorane and decapitation, blood was drawn in an EDTA tube and centrifuged at 1000 ×*g* for 10 min at 4 °C. The supernatant was aliquoted and stored at −80 °C until further analysis.

2.3. Adeno-associated viral (AAV) production and injection in SOD1^{G93A} transgenic mice

The cDNA encoding the extracellular domain of Nrg1 type III isoform (Nrg1-III) was kindly provided by G. Corfas (University of Michigan, Ann Arbor, MI). The sequence was cloned between AAV2 ITRs and was under the regulation of the CMV promoter. The woodchuck hepatitis virus responsive element (WPRE) was added at the 3′ end to stabilize mRNA expression (Loeb et al., 1999). AAVrh10 viral stocks were produced by the Viral Production Unit of Universitat Autònoma de Barcelona (http://viralvector.eu) as previously described (Zolotukhin et al., 1999), by triple transfection into HEK293-AAV cells of the expression plasmid, Rep2Caprh10, containing AAV genes (kindly provided by J.M. Wilson, University of Pennsylvania, Philadelphia, PA) and pXX6 plasmid containing adenoviral genes (Xiao et al., 1998), needed as helper virus. AAV particles were purified by iodixanol gradient. Titration was evaluated by picogreen (Invitrogen) quantification (Piedra et al., 2015) and calculated as viral genomes per milliliter (vg/mL). Serotype-matching AAVrh10 empty vector was used as a control (mock).

AAV intrathecal administration was performed as previously described (Homs et al., 2014). Briefly, eight 8-week-old SOD1^{G93A} mice were anesthetized by intraperitoneal administration of ketamine (10 mg/kg; Imalgene; Merial Laboratories) and xylacine (1 mg/kg; Rompun; Bayer AG). After exposing the lumbar L3 and L4 vertebrae, 7.6×10^{10} vg of an AAV, encoding the extracellular domain (ECD) of Nrg1 type III (AAV-Nrg1.III) in a total volume of 10 µl, were slowly delivered into the intervertebral foramen using a Hamilton syringe and a 33-Gauge needle (Hamilton Company). Proper position of the needle was confirmed by a tail flick reflex. The needle was removed 30 seconds after the end of vector delivery to favor spread through the CSF and avoid efflux. After injection, paraspinal muscles were sutured and the skin closed with suture clips. All mice were fed *ad libitum* with a standard diet (Teklad Global, Harlan Teklad). Plasma samples were obtained at sacrifice, 8 weeks after the intrathecal AAV-Nrg1.III administration.

2.4. Protein extraction from brains of SOD1^{G93A} mice

For analysis of the proteolytic processing of ErbB4 in the SOD1^{G93A} mice, the brains from six 12-week-old transgenic mice and five wild-type littermates were removed and the cerebral hemispheres were dissected out, discarding the brainstem and cerebellum. Both brain hemispheres were homogenized with a Dounce-type glass homogenizer in ice-cold buffer containing 10 mM Hepes pH 7.5, 1.5 mM $MgCl_2$, 10 mM KCl, 1 mM $NaVO_4$, 25 mM NaF, 200 mM sucrose, 10% NP-40 (*w/v*), 0.5 mM PMSF (phenylmethylsulfonyl fluoride), 5 mM PNT (1,10-Phenanthroline monohydrate from Sigma-Aldrich Co) and supplemented with protease inhibitor (Roche). Then, the homogenates were sonicated and frozen at −80 °C until use. Total protein concentrations were determined using the bicinchoninic acid method (BCA from Pierce).

2.5. HEK293 cells and ErbB4/Nrg1 over-expression

HEK293 cells (1.5×10^6 cells/well) were grown in 60 mm plates in Dulbecco's modified Eagle's medium (DMEM; Sigma-Aldrich Co) supplemented with 5% fetal bovine serum (FBS; Gibco) and 100 µg/mL penicillin/streptomycin (Gibco). After 24 h, the medium was collected and cells washed twice with phosphate buffered saline (PBS) and then transferred to modified Eagle's Minimum Essential Media (OptiMEM; Gibco), supplemented with glutamine (2 mM), which allow maintenance of cells without serum. Cells in OptiMEM were transfected with a construct encoding full-length ErbB4 JM-a splicing variant (Gambarotta et al., 2004), susceptible to metalloprotease/secretase proteolytic processing (Määttä et al., 2006); and alternatively co-transfected with a plasmid encoding for the ECD of Nrg1-III (EF1-Nrg1a Type III Flag), using Lipofectamine 2000 (Thermo Fisher Scientific), according to the manufacturer's instructions. Cell medium was changed and, after 48 h of transfection, cells were mechanically lysed in cold lysis buffer [50 mM Tris-HCl pH 7.4, 150 mM NaCl, 2 mM EDTA, 1% NP-40, 1 mM PMSF supplemented with phosphatase and protease inhibitors (Roche)], incubated for 30 min on ice, centrifuged for 10 min (10,000 rpm, 4 °C) and the supernatant fraction was kept. The conditioned medium was supplemented with PMSF inhibitor (1 mM), centrifuged at 1000 rpm for 5 min at RT, and concentrated using Amicon® Ultra 10 K filters (EMD Millipore), according to the manufacturer's instructions. Both, cell lysates and conditioned media were analyzed by western blotting.

2.6. Detection of ErbB4 by western blotting and immunoprecipitation

For western blotting, CSF (30 µL) and plasma samples (0.4 µL), mouse brain extracts (40 µg), HEK293 extracts (25 µg) and supernatant fractions (25 µL) were denatured at 65 °C for 5 min and resolved by electrophoresis on 10% SDS-polyacrylamide gels. Following electrophoresis, proteins were blotted onto nitrocellulose membranes (Bio-Rad Laboratories, Inc.). ErbB4 was detected with antibodies against the N-terminal part, a polyclonal antibody (from Thermo Fisher Scientific Inc.), the immunogen of which is a synthetic peptide between 25 and 35 amino acids from the N-terminal region of human ErbB4; a monoclonal ErbB4 antibody (clone Ab77; Thermo Fisher Scientific Inc.), the immunogen of which is an extracellular fragment of recombinant human ErbB4; or an antibody against the C-terminal part of the protein (polyclonal antibody C-18 from Santa Cruz). GAPDH (Ambion, Life Technologies) was used as a loading control for brain and cellular extracts. All samples were analyzed at least in duplicate in independent aliquots to avoid thawing-freezing cycles. Ponceau staining served to monitor potential loading inaccuracies in individual blots of CSF and plasma samples, and cell media samples, in which equal volumes were loaded. Antibody binding was visualized with fluorescent secondary IRDye antibodies and recorded on an Odyssey CLx Infrared Imaging system (LI-COR Biosciences GmbH).

Immunoprecipitations were performed at 4 °C by incubating 200 µL of CSF or 2 µL of plasma, overnight with the polyclonal ErbB4 antibody, or alternatively as a control with an irrelevant rabbit IgG, both previously coupled to protein A-Sepharose by Dimethyl pimelimidate dihydrochloride (Sigma-Aldrich Co). After incubation, the resin was washed with PBS and eluted with 0.1 M glycine buffer at pH 2.5. Separated proteins were subjected to SDS-PAGE, transferred to nitrocellulose membranes and analyzed by western blotting using the monoclonal N-terminal antibody.

2.7. Enzymatic deglycosylation

Human serum samples were treated with an enzymatic deglycosylation kit from ProZyme (GK80110) following manufacturer indications, and then subjected to SDS-PAGE and western blot analysis. This treatment removes all *N*-linked glycans and simple *O*-linked glycans

(including polysialylated) from glycoproteins. After treatment, samples were analyzed by western blotting.

2.8. Mass spectrometric data analysis

Immunoprecipitation was also performed for high-resolution mass spectrometry analysis of CSF ErbB4. For this purpose, immunoprecipitation (IP) of 5 mL of human CSF was performed using a KingFisher magnetic particle processor (Thermo Fisher Scientific Inc.), according to a previously described protocol (Portelius et al., 2010) with minor modifications. The polyclonal ErbB4 antibody was again used to immunoprecipitate ErbB4. Briefly, 4 µg of the antibody was cross-linked to 50 µL magnetic Dynabeads M-280 sheep anti-mouse IgG (Invitrogen). Beads with antibodies were incubated in CSF overnight. Eluates (100 µL in 0.5% formic acid) were vacuum-dried and stored at −80 °C.

Then, immunoprecipitated samples were digested in solution with trypsin (Sequencing grade modified trypsin, Promega, Madison, WI) as follows: the dried eluates were dissolved in 25 µL of 50 mM ammonium bicarbonate (Riedel-de Haën, Seelze, Germany) and shaken for 1 h. Proteins were reduced by adding 5 µL of 20 mM dithiothreitol (Sigma-Aldrich) in 50 mM ammonium bicarbonate, followed by incubation 30 min at 60 °C. The solutions were cooled to room temperature and the proteins were alkylated by adding 5 µL of 75 mM iodacetamide (Sigma-Aldrich) in 50 mM ammonium bicarbonate followed by incubation 30 min in darkness. One µg trypsin was dissolved in 400 µL 50 mM ammonium bicarbonate (pH 8.5). Five µL trypsin solution was added followed by incubation overnight at 37 °C. To stop the enzymatic activity, 2 µL of 10% aqueous trifluoroacetic acid (Sigma-Aldrich) were added followed by incubation 45 min at 37 °C, after which the solution was centrifuged 10 min at 16910 ×*g*. Samples were then vacuum-dried and stored at −80 °C pending mass spectrometric analysis.

Mass spectrometric analysis was performed using a Dionex 3000 nanoflow LC system coupled to a Q Exactive (both Thermo Fisher Scientific), a hybrid electrospray ionization linear quadrupole–Orbitrap mass spectrometer. Briefly, a reversed phase Acclaim PepMap C18 (100 Å pore size, 3 µm particle size, 20 mm length, 75 µm i.d., Thermo Fisher Scientific) trap column was used for online desalting and sample clean-up, followed by a reversed phase Acclaim PepMap RSLC C18 (100 Å pore size, 2 µm particle size, 75 µm i.d., 150 mm length, Thermo Fisher Scientific) for separation. The separation was performed at a flow rate of 300 nL/min by applying a linear gradient of 0–40% B for 50 min. Mobile phase A was 0.1% formic acid in water (*v*/v) and mobile phase B was 0.1% formic acid and 84% acetonitrile in water (v/v/v). All mass spectra were acquired data dependent in positive ion mode with a resolution setting of 70,000 for precursor ion acquisitions and 17,500 fragment mass spectra. Precursor fragmentation was obtained by higher energy collision induced dissociation (HCD) using a normalized collision energy (NCE) setting of 28. Database searches were performed for screening purposes using Proteome Discoverer (v.2.1, Thermo Fisher Scientific) and submitted to an in-house Mascot database server (v.2.6, Matrix Science, London, UK). Spectra were searched against a Uniprot human database using 10 ppm mass accuracy for precursor ions and 50 mDa for fragment ions.

2.9. Statistical analyses

All results are presented as the mean ± SEM. All data were analyzed using SigmaStat (Version 2.0; SPSS Inc.), either by one-way analysis of variance (ANOVA), or by a Student's *t*-test (two-tailed) for single pair-wise comparisons, determining the exact *p* values. When normality was rejected, a Mann-Whitney Rank Sum Test was used. Correlations between variables were assessed by linear regression analyses. A p value $< .05$ was considered significant.

3. Results

3.1. Ecto-ErbB4 fragments are present in CSF and plasma

ErbB4 is a 1308 amino-acid residue type I glycoprotein with extracellular and intracellular domains of similar size (Fig. 1A). To determine whether ecto-ErbB4 is present in human CSF, we first examined the samples by immunoprecipitation/western blot analysis using a polyclonal anti-N-terminal antibody. Several immunoreactive bands for the N-terminus of ErbB4, between 55 and 80 kDa, were detected in human CSF (Fig. 1B). CSF samples were also immunoprecipitated using the polyclonal anti-ErbB4 antibody, and mass spectrometric analysis identified eighteen tryptic peptides spanning amino acids 36–606 of human ErbB4 (Uniprot entry Q15303, ERBB4_HUMAN) in CSF, matching sequences located in the N-terminal ectodomain (Fig. 1A and Supplementary Table 1). Western blot analysis of the immunoprecipitates with an alternative anti-N-terminal monoclonal antibody confirmed that the 55 kDa and 80 kDa bands were ectodomain fragments of ErbB4 (Fig. 1B). An 80 kDa band was also observed in the unbound fraction. The unbound fraction was rich in a non-specific 70 kDa band which displayed positive immunoreactivity to an anti-albumin antibody (not shown). The 55 and 80 kDa bands were not observed in negative immunoprecipitation controls with an irrelevant antibody (Fig. 1B).

The ecto-ErbB4 fragments were also detected in human plasma. The smallest fragments in plasma were resolved as a doublet of bands between 55 and 50 kDa (Fig. 1C). Both of these ecto-ErbB4 fragments were also observed in immunoprecipitates, while the 80 kDa band was not present (Fig. 1C). To assess whether this small ecto-ErbB4 doublet represented two different glycoforms of the same fragment, we determined the effect of enzymatic deglycosylation on the electrophoretic migration of ecto-ErbB4 fragments in human plasma. After treatment with glycosidases, the molecular masses were lower with reduction in apparent molecular mass but a doublet was still seen, indicating that original differences in molecular mass were not due to differences in glycosylation (Fig. 1D). These 50–55 kDa ecto-ErbB4 fragments were also detected in freshly collected human CSF and plasma samples (Supplementary Fig. 1), indicating that these fragments are not artefactual proteolytic fragments originating during storage of the samples.

In mouse plasma, the small ecto-ErbB4 doublet was also apparent, but poorly resolved in most samples (Fig. 2A). The doublet was the only immunoreactive band absent in plasma from ErbB4 knockout mice (Tidcombe et al., 2003), which displayed weak immunoreactivity for an 80 kDa band (Fig. 2A).

Moreover, to confirm the specificity of the staining of the short 55 ecto-ErbB4 fragment and to determine whether this fragment is generated subsequently to the binding of neuregulins, we first over-expressed ErbB4 in the HEK293 cells and examined whether Nrg1 induces the generation of the 55 kDa ecto-ErbB4 fragment. HEK293 cells, maintained in OptiMEM medium (to avoid the interference of albumin) were transfected with a construct encoding the full-length cleavable ErbB4 JM-a splicing variant (Gambarotta et al., 2004). The over-expression of ErbB4 in HEK293 cells induced the generation of the full-length protein as well as C-terminal fragments in cell homogenates, and both larger and short ecto-ErbB4 fragments in the cell medium (Fig. 2B). HEK293 cells co-transfected with a construct encoding for the ECD of Nrg1-III showed increased generation of shorter ecto-ErbB4 fragments in the cell medium (4.5 times higher immunoreactivity levels compared with levels determined in cells transfected only with ErbB4, $n = 3$ for each condition; $p = 007$; Fig. 2B).

Altogether, our results confirm the presence of circulating shortest ecto-ErbB4 fragments of ~55 kDa. The immunoreactivity of the larger 80 kDa band overlaps partially with unspecific reactivity, at least in plasma samples, a fact that can compromise a reliable quantification.

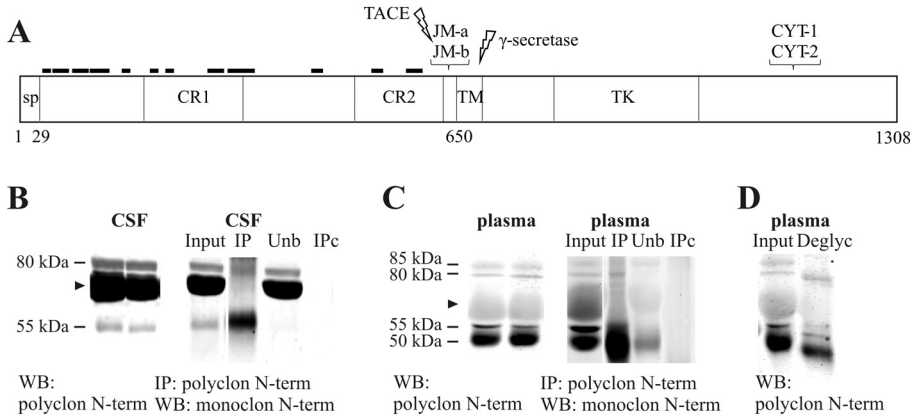

Fig. 1. Ecto-ErbB4 fragments are present in CSF and plasma. (**A**) Schematic representation of ErbB4 including domain organization (adapted from (Hollmén et al., 2012; Zeng et al., 2007). The ErbB4 glycoprotein is a type I transmembrane receptor tyrosine kinase consisting of 1308 amino acids and exhibiting a molecular mass of ~160–180 kDa depending on the degree of glycosylation. ErbB4 possesses an extracellular region containing two extracellular cysteine-rich (CR1 and CR2) domains, a transmembrane domain (TM) flanked by short intracellular juxtamembrane (JM) regions. The extracellular domain contains alternative JM isoforms, with a proteolytic TACE cleavage site between His-651 and Ser-652 in JM-a but not in JM-b. The approximate cleavage site by γ-secretase is also indicated. The intracellular region including a tyrosine kinase domain, a regulatory domain with autophosphorylation sites plus sequence changes attributable to the CYT-1 and CYT-2 isoforms (CYT-2 isoform has a 16-amino acid deletion that contains a PI3K-binding and a WW domain binding motif) and the carboxyl-terminal tail are also shown. The approximate locations of CSF-ADAM10 peptides identified by mass spectrometry are indicated (Hansson et al., 2017). (**B**) Western blot of human CSF samples from control subjects. Control CSF samples were also immunoprecipitated and precipitated (IP) and unbound proteins (Unb) were immunoblotted with the indicated anti-ErbB4 antibodies, or resolved by mass spectrometry. Eighteen tryptic peptides spanning amino acids 36–606, *i.e.*, most of the N-terminal half of ErbB4 (Uniprot entry Q15303, ERBB4_HUMAN), were detected with high confidence (see above for approximate locations and supplemental Table 1 for details). Extracts incubated with a rabbit IgG (IPc) were analyzed in parallel as negative controls. Arrowhead indicates a non-specific band. (**C**) Control human plasma samples were also resolved by western blotting and immunoprecipitated as indicated. (**D**) Additionally, human samples were resolved by SDS-PAGE prior to and after enzymatic deglycosylation (deGlyc).

3.2. Ecto-ErbB4 fragments are decreased in CSF and plasma of ALS and ALS-FTD patients

To assess whether levels of ecto-ErbB4 fragments are altered in ALS and ALS-FTD subjects, we first analyzed CSF samples from 30 ALS patients, including 10 ALS-FTD, and 13 age-matched controls. The 80 and 55 kDa ecto-ErbB4 fragments were detected with the polyclonal N-terminal antibody in all CSF samples analyzed (Fig. 3A). Considering the previous analyses of specificity, we focused on the immunoreactivity of the short 55 kDa band, which was found decreased (34%; $p = .036$) in patient samples compared to controls (Fig. 3B). The decrease was particularly marked for the ALS-FTD patients (39%; $p = .038$) than for the ALS alone subjects (31%; $p = .078$). The large 80 kDa ecto-ErbB4 fragment was also significantly decreased (24%; $p = .021$), to a similar extent in the ALS group without concomitant FTD (21%; $p = .044$) and in the ALS-FTD subjects (29%; $p = .042$), compared to controls (Fig. 3B). The immunoreactivity levels of the 80 and the 55 kDa ecto-ErbB4 fragments were correlated in the controls ($R = 0.85$; $p < .0001$) and ALS samples ($R = 0.57$; $p < .0001$).

In the human plasma samples (from the same individuals, except for one ALS subject), it was possible to discriminate and quantify separately the 50 and 55 kDa doublet band (Fig. 4A). Levels of the 50 and 55 kDa bands appeared to correlate in the control samples ($R = 0.50$; $p = .081$), but did not correlate in ALS samples ($R = 0.008$; $p = .97$). The immunoreactivity for the ~50 kDa band did not differ between ALS and control subjects; while, in agreement with the changes found in CSF, for the 55 kDa band there was a significant decrease in the ALS group (45%; $p = .004$) compared with the controls (Fig. 4B). When analyzed separately in the sub-groups of pathological samples, the decrease was significant for both ALS-FTD (47%; $p = .006$) and ALS patients (43%; $p = .017$). The largest ecto-ErbB4 fragments were also resolved as a ~80 and 85 kDa doublet, which did not show significant changes between groups (Fig. 4B). Levels of the 80–85 kDa doublet correlated within the control group ($R = 0.59$; $p = .034$), but not in the ALS group ($R = 0.29$; $p = .13$). No significant correlations were observed between the largest and the shortest ecto-ErbB4 fragments in plasma from control or ALS subjects (not shown).

No relationship was observed in the ALS patients in the levels of CSF or plasma ecto-ErbB4 fragments between the bulbar or spinal onset subsets. Although the groups were not balanced regarding gender, we did not observe differences in ecto-ErbB4 levels between males and females in the ALS group. Levels of CSF or plasma ecto-ErbB4 fragments did not correlate with age. In the ALS patients, no correlation was evident between CSF or plasma ecto-ErbB4 fragments and age of appearance of motor symptoms or time delay from onset to lumbar puncture. In those ALS patients who died, no correlations were observed with the survival time.

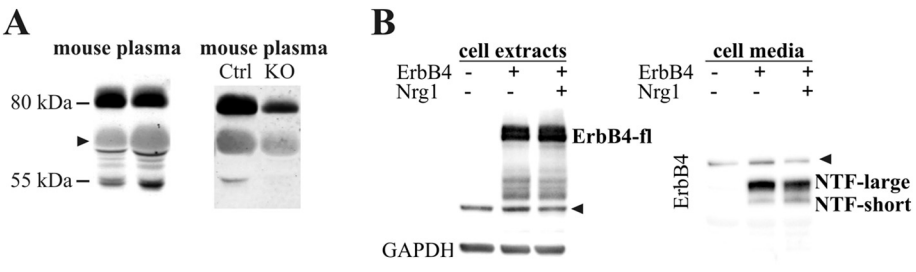

Fig. 2. Shortest ecto-ErbB4 fragments are specific and generated in presence of Nrg1. (**A**) Plasma samples from wild-type mice were blotted with a polyclonal anti-N-terminal ErbB4 antibody. ErbB4-KO mice (KO) and control littermates (Ctrl) were also blotted with the same ErbB4 antibody. In general, immunoreactivities of the bands corresponding to largest ecto-ErbB4 complexes were weaker in ErbB4-KO mice than in control littermates, but the shortest bands were absent. (**B**) HEK cells were transfected with the full-length cleavable ErbB4 JM-a (ErbB4), and and/or with ECD human Nrg1-III (Nrg1). ErbB4 in the cell extracts and soluble ErbB4 in the medium were assayed in western blots using anti C-terminal or N-terminal polyclonal antibodies respectively (equivalent amounts of protein of the cell extracts and equal volumes of medium were loaded in each lane). GAPDH served as a loading control for cellular extracts and Ponceau staining also served to check for potential loading inaccuracies of cell medium. The C-terminal antibody served to confirm ErbB4 over-expression in transfected cells (ErbB4 full-length: ErbB4-fl). The N-terminal antibody detects the largest (NTF-large) and shortest (NTF-short) soluble N-terminal fragments in cellular medium. A representative blot from three independent experiments is shown. Arrowhead indicates non-specific bands.

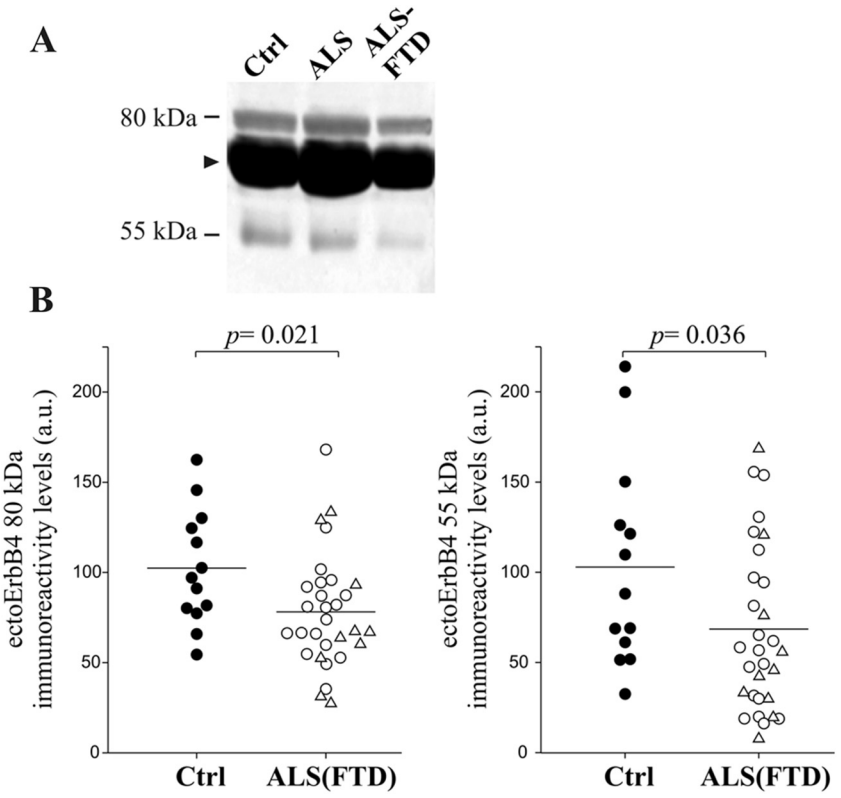

Fig. 3. Decreased ecto-ErbB4 fragments in ALS CSF. (**A**) Representative blot human CSF samples probed with the polyclonal anti-N-terminal ErbB4 antibody, and (**B**) densitometric quantification of the immunoreactive ~80 and 55 kDa ecto-ErbB4 fragments in CSF samples from 20 ALS (open circle), 10 ALS with concomitant FTD (ALS-FTD; open triangle) and 13 age-matched control subjects (Ctrl; closed circle). Equal volumes of CSF were loaded in each lane and Ponceau staining served to monitor potential loading inaccuracies (none of the major bands detected by Ponceau staining displayed significant differences between groups). Arrowhead indicates a non-specific band. The figure shows the means ± SEM; *p* values are also shown.

3.3. Ecto-ErbB4 fragments are decreased in plasma of ALS transgenic mice

To determine whether pathogenic mutations associated to ALS may influence the levels of ecto-ErbB4, we examined plasma samples from 12 weeks-old SOD1^{G93A} transgenic mice and littermates by western blotting (Fig. 5A). In mouse plasma, the ~80 kDa band overlapped in size with a band of non-specific immunoreactivity (see Fig. 1E); thus it was not possible to discern if the largest ecto-ErbB4 fragment was affected or not, and for further analysis in the ALS transgenic mouse model, we only quantified the shortest ecto-ErbB4 fragment.

Immunoblotting with the N-terminal ErbB4 antibody revealed lower levels of the shortest ecto-ErbB4 doublet in the plasma of SOD1^{G93A} mice (n = 10; 52% decrease; p = .006) compared to samples of control littermates (n = 10) (Fig. 5A). In mouse plasma, it was not possible to discriminate and quantify the doublet of 50 and 55 kDa bands separately.

Similarly, we found that plasma levels of the short ecto-ErbB4 levels were lower for the ALS transgenic model TDP-43^{A315T} (n = 7; 55% decrease; p = .012) compared with those determined in littermates (n = 10) (Fig. 5B).

3.4. Impaired generation of ecto-ErbB4 fragments in ALS transgenic mice

We have inferred from the *in-vitro* cell model overexpressing Nrg1 and ErbB4 that Nrg1 binding induces the generation of short ecto-ErbB4 fragments. To address further the relation of shortest ecto-ErbB4 fragments with Nrg1 in an *in-vivo* model, we performed intrathecal injections of AAVs encoding the extracellular domain (ECD) of Nrg1 in the SOD1^{G93A} transgenic mice. We found a positive correlation between the levels of soluble Nrg1 and shortest ecto-ErbB4 fragments in the plasma of injected Nrg1-ECD SOD1^{G93A} mice (R = 0.80, p = .018; Fig. 5C, D).

Finally, we examined whether decreased plasma ecto-ErbB4 fragments in the SOD1^{G93A} transgenic mice, which may represent a readout of impaired Nrg1/ErbB4 signaling function, is a direct consequence of decreased ErbB4 expression. Indeed, a significant decrease in ErbB4 mRNA and protein in muscle tissue of ALS patients has been reported (Mancuso et al., 2016) as well as in motor neurons of transgenic SOD1^{G93A} mice (Lasiene et al., 2016). Thus, we determined the levels of unprocessed full-length ErbB4 (ErbB4-fl) and intracellular fragments in brain as an indicator of an alteration on the processing rate of the receptor and potential impairment in ErbB4 signaling. The ErbB4-fl and the intracellular C-terminal fragments (CTF) were resolved and quantified in brain extracts from littermate controls and from transgenic SOD1^{G93A} mice (Fig. 6). We found a decreased ErbB4-CTF/ErbB4-fl ratio in SOD1^{G93A} mice without significant changes in ErbB4-fl, suggesting decreased proteolytic processing of ErbB4.

4. Discussion

Ligand binding to ErbB4 initiates phosphorylation-dependent signaling cascades, but also releases soluble extracellular (ecto-ErbB4) and intracellular (ErbB4-ICD) fragments, similar to the proteolytic processing observed for Notch receptors (De Strooper et al., 1999), the ApoE/reelin receptor ApoER2 (Balmaceda et al., 2014), and other type-I membrane receptors. The ectodomain cleavage of ErbB4 by TACE (Vecchi et al., 1996) occurs between His-651 and Ser-652, placing the cleavage site within the ectodomain stalk region approximately 8 residues prior to the transmembrane domain, resulting in production of a ~80 kDa molecular mass fragment (Cheng et al., 2003). In ErbB4 immunoprecipitates from human CSF, we have identified by mass spectrometry peptide fragments from Leu-36 to Lys-606, and by immunoblotting bands of 80 kDa and 50–55 kDa. Interestingly, the 50–55 kDa ecto-ErbB4 fragments were absent in plasma from ErbB4 knockout mice, indicating that they are authentic ErbB4-derived fragments. The presence of these soluble ErbB4 fragments in cells overexpressing the ErbB4-JM-a and the ligand Nrg1, as well as in AAV-Nrg1 SOD1^{G93A} mice, suggests that cleavage of ErbB4 and generation of these shortest fragments occur in response to ligand binding. Analysis of CSF/plasma samples from patients with loss-of-function mutations in ErbB4 associated with ALS but also with other pathological conditions, such as

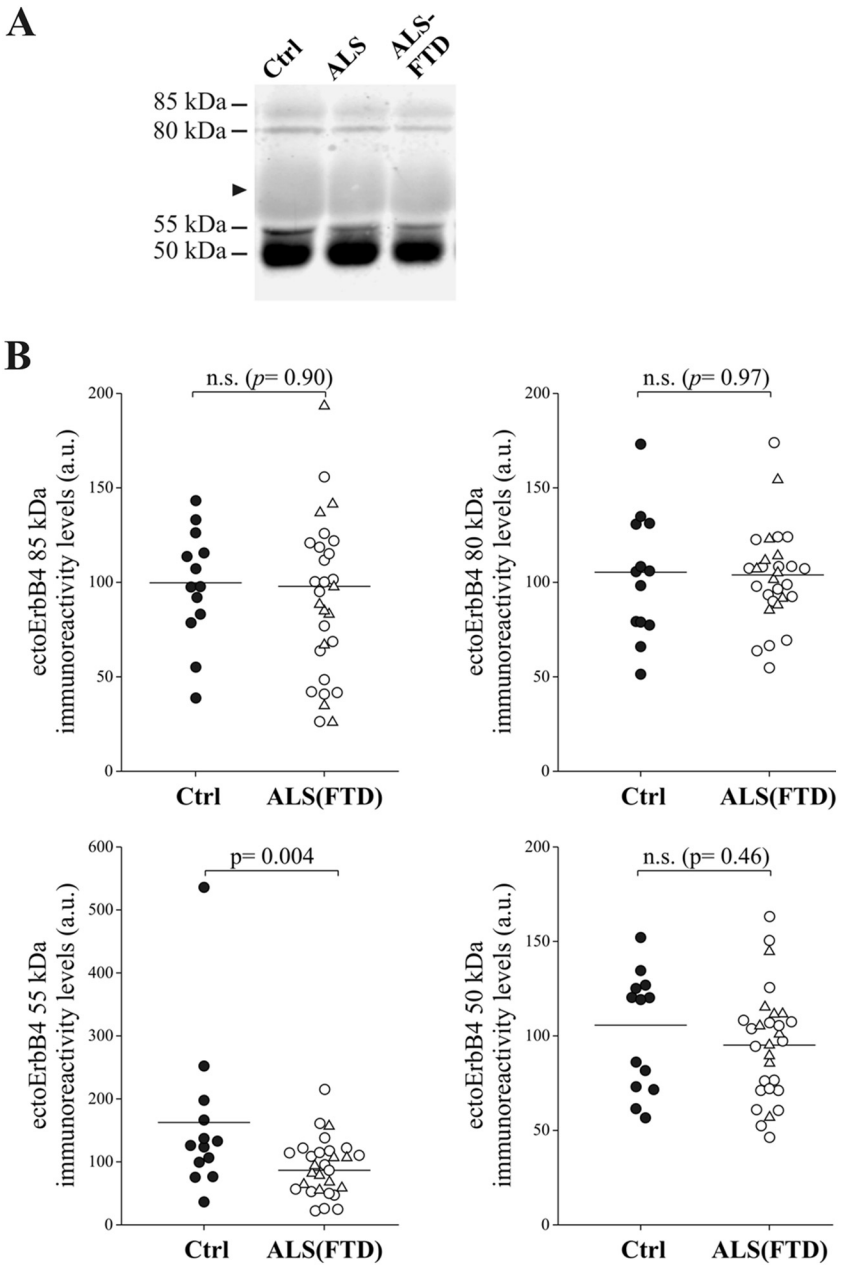

Fig. 4. Decreased ecto-ErbB4 fragments in ALS plasma. (**A**) Representative blot of human plasma samples probed with anti-N-terminal ErbB4 antibody, and (**B**) densitometric quantification of the immunoreactive ~85, 80, 55 and 50 kDa ecto-ErbB4 fragments in plasma samples from the same individuals shown in Fig. 3, 19 ALS (open circle), including 10 ALS with concomitant FTD (ALS-FTD, open triangle) and 13 age-matched control subjects (Ctrl; closed circle). Equal volumes of plasma were loaded in each lane and Ponceau staining served to monitor potential loading inaccuracies. Arrowhead indicates a non-specific band. The figure shows the means ± SEM; *p* values are also shown (n.s.: non-significant).

in several types of cancer (Tvorogov et al., 2009), should serve to strengthen the link between ErbB4 activity and production of ecto-ErbB4 fragments.

In this study, the analysis of the ecto-ErbB4 fragments in CSF by western blotting showed a decrease in the 80 kDa and 55 kDa bands in ALS and ALS-FTD patients, being the decrease in the 55 kDa band more pronounced in the ALS-FTD subgroup. In plasma samples from the same subjects, and from $SOD1^{G93A}$ and $TDP\text{-}43^{A315T}$ transgenic mice, the decrease was only significant for the 55 kDa band. However, quantification of the 80 kDa band was less reliable, at least in plasma, because of overlap with a nonspecifically stained band. Accordingly, we focused our analysis on the shortest ecto-ErbB4 fragments.

It is currently not known how the shortest ecto-ErbB4 fragment identified in CSF and plasma is generated. Internal control experiments helped rule out the possibility that this short ecto-ErbB4 fragment is a proteolytic artefact originating during storage or handling of the samples; moreover this fragment was also present in freshly collected CSF and plasma samples. In addition to the ErbB4 metalloprotease cleavage and non-cleavage splicing variants JM-a and JM-b, splicing at the cytoplasmic (CYT) locus produces the minor CYT-1 and major CYT-2 variants, respectively, differing only in 16 amino acids as a result of exon skipping in CYT-2 (Junttila et al., 2000). Thus, alternative splicing does not explain differences in ErbB4 fragments molecular mass, since it would result only in a minor shift of the CTF and ICD. Moreover, cleavage of ErbB4 by TACE or an alternative metalloprotease is expected to occur in a similar position since similar ErbB4-CTFs have been identified (Gambarotta et al., 2015; Lee et al., 2002). Nevertheless, ErbB4-ICD fragments of ~50 kDa have been described in anaplastic large-cell lymphoma cells, highly correlating with MMP9 levels (Scarfò et al., 2016), a matrix metalloproteinase that can regulate kinase pathways through ErbB receptors (Chattopadhyay and Shubayev, 2009). A ~50 kDa ErbB4-ICD, among other small C-terminal fragments, has been also identified in human and in non-human primate brain homogenates and in nuclear extracts (Chong et al., 2008), suggesting further or alternative processing of ErbB4 fragments and their functional capacity in the brain (Thompson et al., 2007). Since multiple proteolytic events allow the release of extracellular and cytoplasmic fragments of transmembrane receptors (reviewed in Lichtenthaler et al.,

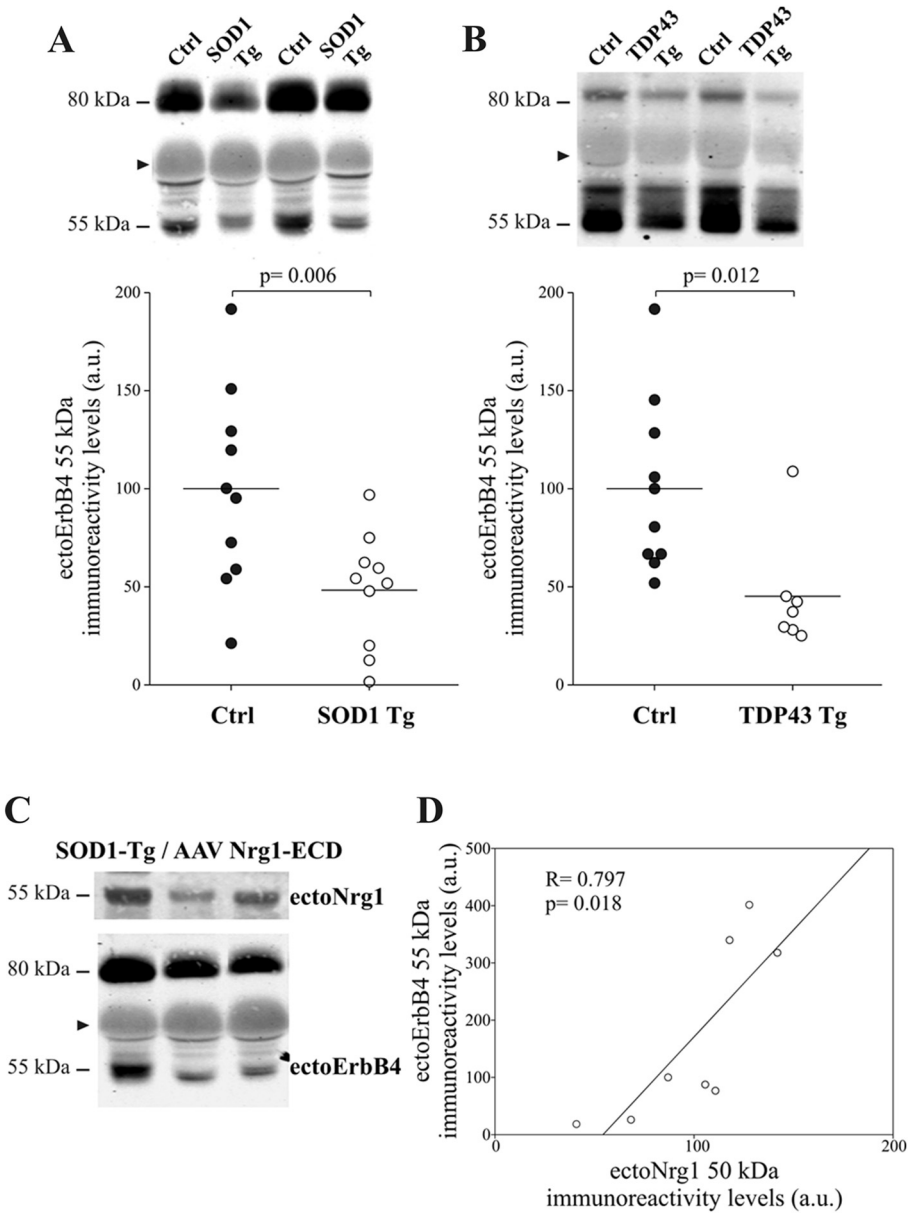

Fig. 5. Decreased levels of 55 kDa ecto-ErbB4 fragments in plasma from ALS transgenic mice. (**A**) Representative blot and densitometric quantification of the 55 kDa ecto-ErbB4 band in plasma samples from 12-weeks-old SOD1^{G93A} transgenic (SOD1 Tg; $n = 10$; open circle) and wild-type littermates (Ctrl; $n = 10$; closed circle) animals. (**B**) Representative blot and densitometric quantification of the 55 kDa ecto-ErbB4 band in plasma samples from 12-weeks-old TDP-43^{A315T} transgenic (TDP-43 Tg; $n = 7$; open circle) and wild-type littermates (Ctrl; $n = 10$; closed circle) animals. Equal volumes of plasma were loaded in each lane and Ponceau staining served to monitor potential loading inaccuracies. Arrowhead indicates a non-specific band. The figure shows the means ± SEM; p value is also shown. (**C**) Eight-weeks-old SOD1-Tg ($n = 8$) were injected with an AAV encoding the ECD of Nrg1-III and then the plasma levels of Nrg1-III (ecto-Nrg1) and ecto-ErbB4 fragments were analyzed after euthanasia at 16-weeks of age; (**D**) showing a positive correlation. Linear regression coefficient (R) and p value are shown.

2018), alternative or further processing of the ecto-ErbB4 cannot be discarded.

Considering that doublets of ecto-ErbB4 fragments are detectable only in plasma and not in CSF, and since the pair of bands are differentially separated during electrophoresis in human and mouse plasma, we examined whether these differences in electrophoretic migration may be due to differences in glycosylation. Different cell types glycosylate proteins specifically and differentially, and glycoforms (and derived fragments) can exhibit differences in apparent molecular mass (Thomson et al., 2016). However, after enzymatic deglycosylation, the doublet band of the shortest ecto-ErbB4 fragments was maintained in human plasma samples. We cannot discard the idea that the 50 and 55 kDa fragments are from different glycoforms of ErbB4, since 85 and 80 kDa seem to be the same proteolytic fragment exhibiting differences in glycosylation. We can only speculate that proteolytic events related to generation of the shortest ErbB4 fragments, may depend on glycosylation and/or cellular origin. Interestingly, it has been shown that glycosylation can modulate processing of ErbB4 by specific ADAM species (Goth et al., 2015).

In human plasma, in which it was possible to better discriminate the doublet of 50 and 55 kDa ecto-ErbB4 fragments, only the 55 kDa one was altered in ALS patients. The 55 kDa band from plasma was the only one, and not the 50 kDa, which correlated with the unique short ecto-ErbB4 fragment detected in CSF. Accordingly, we assume that ErbB4 processing (and signaling) is not affected to the same degree in all tissues during the progression of ALS. ErbB4 is likely to be the major mediator of Nrg1 function in the brain (Falls, 2003; Wen et al., 2010). Indeed, our data indicate that in CSF the largest change occurs in ALS patients suffering from FTD. Further studies should clarify also if levels of ecto-ErbB4 are also altered in the CSF of patients with FTD without concomitant occurrence of ALS.

Our data, from ALS and ALS-FTD subjects and ALS transgenic mice models, suggest that levels of ErbB4 proteolytic fragments can be a suitable read-out of impaired ErbB4 signaling. We cannot discard the possibility that decreased levels of circulating ecto-ErbB4 fragments reflect decreased expression levels of ErbB4 previously described in muscle tissue from ALS patients (Mancuso et al., 2016), and muscle and motor neurons of transgenic SOD1^{G93A} mice (Lasiene et al., 2016; Mancuso et al., 2016). However, in TDP-43-knockdown neurons, although total ErbB4 protein levels are similar, the surface expression and

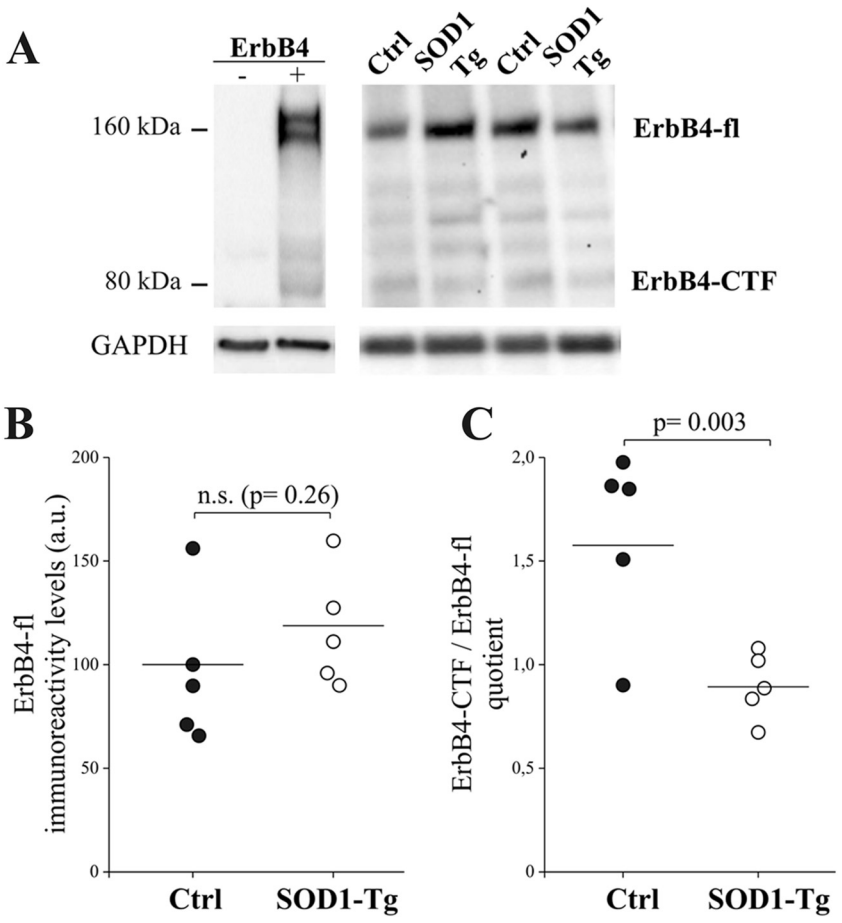

Fig. 6. Decreased generation of C-terminal ErbB4 fragments in brains of SOD1^{G93A} transgenic mice. (**A**) CHO cells were transfected with ErbB4 (+) or with the pcDNA3 expression plasmid as a control (−) and resolved with a C-terminal antibody for ErbB4 in order to resolve the C-terminal fragment of ErbB4 (ErbB4-CTF). Western blots of brain extracts from 12-weeks-old transgenic mice (SOD1-Tg; $n = 5$; open circle) and wild-type littermates (Ctrl; $n = 5$; closed circle) were also probed for ErbB4 C-terminal and GAPDH immunoreactivities. (**B**) Densitometric quantification of the full-length ErbB4 (ErbB4-fl; ~160 kDa) was normalized to GAPDH staining intensity. (**C**) The quotient derived from the ErbB4-CTF immunoreactivity (~80 kDa) relative to that for the ErbB4-fl in each sample [ErbB4-CTF/ErbB4-fl] reflects altered proteolytic processing of ErbB4 in SOD1-Tg. The figure shows the means ± SEM; p values are also shown.

activity of ErbB4 is reduced, indicating a compromise in the Nrg1/ErbB4 pathway in animal models of ALS (Schwenk et al., 2016). In this study, full-length ErbB4 levels in cortical extracts from SOD1^{G93A} mice were not significantly different from controls, indicating that decreased ErbB4-CTFs were not a consequence of changes in total ErbB4. Therefore, our data suggest that decreased circulating ecto-ErbB4 fragments reflect, at least in part, an impaired Nrg1/ErbB4 activity in ALS. It would be also interesting to determine whether changes in the activity of specific metalloproteases occur during the ALS progression and can contribute to the detected changes, perhaps affecting other proteins in addition to ErbB4.

Whether the decrease in ErbB4 proteolytic processing depends on reduced levels of specific subtypes of neuregulins or alternative ligands, or interference with other proteins or pathological processing, will require future investigation. In any case, we propose that quantifying the circulating ecto-ErbB4 fragments may be useful to estimate impaired ErbB4 signaling in ALS and ALS-FTD subjects. However, the large overlap of ecto-ErbB4 fragment levels between controls and ALS/ALS-FTD limits their potential use as a diagnostic biomarker, at least using a western blotting approach. Despite substantial efforts, no biomarkers have been identified to facilitate early diagnosis in ALS patients. In order to define the potential of the ecto-ErbB4 fragment as a biomarker for ALS and/or ALS-FTD, it will be valuable to replicate our present findings using another quantitative assay, such as an enzyme linked immunosorbent assay (ELISA). Previous studies have approached the determination of the levels of ecto-ErbB4 fragments by ELISA in medium of cultured cancer cells (Hollmén et al., 2012, 2009). However, prior to this application, it would be necessary to define if an ELISA designed for diagnostic purposes can discriminate between the largest and shortest ecto-ErbB4 fragments, and, at least in plasma, discriminate between 50 and 55 kDa fragments.

5. Conclusions

In conclusion, we have demonstrated the existence of circulating 55 kDa ecto-ErbB4 fragments, which are decreased in CSF and plasma of ALS, and particularly in ALS-FTD subjects, and may be useful to evaluate *in vivo* ErbB4 signaling. In this regard, determination of circulating ecto-ErbB4 fragments may also be applicable as a read-out biomarker for determining the efficiency of therapeutic agents targeting the Nrg1 receptor. We also present evidence that ErbB4 processing is affected in the brain of an ALS transgenic mouse model, raising possibility that a dysfunctional Nrg1/ErbB4 pathway contributes to some of the complex processes involved in ALS-FTD pathology.

Supplementary data to this article can be found online at https://doi.org/10.1016/j.nbd.2018.12.021.

Acknowledgments

We thank Dr. J. Fernandez-Ruiz (Department of Biochemistry and Molecular Biology, Faculty of Medicine, Complutense University, Madrid, Spain) for providing with the TDP-43^{A315T} mice model. We also thank Drs. B. Rico and C. Bernard (Centre for Developmental Neurobiology, Institute of Psychiatry, Psychology and Neuroscience, King's College London, London, UK) for generously providing plasma samples from the ErbB4-KO mouse. We also thank Dr. G. Corfas (Kresge Hearing Research Institute, The University of Michigan, Ann Arbour, MI, USA) and Dr. G. Gambarotta (University of Torino, Turin, Italy) for kindly providing with Nrg1 type III and erbB4 JM-a plasmids, respectively. We are in debt with Dr. L. Ariza (UAB) for technical assistance.

Funding

This work was supported by grants from the Fondo de Investigaciones Sanitarias (PI15/00665 to JSV and PI15/01618 to RRG), cooperative project 2015-01 from CIBERNED (Instituto de Salud Carlos III, Spain) to XN and JSV, all co-funded by the Fondo Europeo de Desarrollo Regional (FEDER), Unión Europea, "Una manera de hacer Europa"; grants TV3201428-10 to XN and 201437 to RRG of Fundació La Marato-TV3; and grant #20289 of AFM-Telethon to XN. HZ is a Wallenberg Academy Fellow and is supported by grants from the Swedish and European Research Councils and the UK Dementia Research Institute at UCL. KB holds the Torsten Söderberg Professorship in Medicine at the Royal Swedish Academy of Sciences. We also acknowledge financial support from the Spanish Ministerio de Economía y Competitividad, through the "Severo Ochoa" Programme for Centres of Excellence in R&D (SEV-2017-0723).

References

Alcolea, D., et al., 2015. Amyloid precursor protein metabolism and inflammation markers in preclinical Alzheimer disease. Neurology 85, 626–633. https://doi.org/10.1212/WNL.0000000000001859.

Alcolea, D., et al., 2017. CSF sAPPβ, YKL-40, and neurofilament light in frontotemporal lobar degeneration. Neurology 89, 178–188. https://doi.org/10.1212/WNL.0000000000004088.

Ancot, F., et al., 2009. Proteolytic cleavages give receptor tyrosine kinases the gift of ubiquity. Oncogene 28, 2185–2195. https://doi.org/10.1038/onc.2009.88.

Balmaceda, V., et al., 2014. ApoER2 processing by presenilin-1 modulates reelin expression. FASEB J. 28, 1543–1554. https://doi.org/10.1096/fj.13-239350.

Bao, J., et al., 2003. Back signaling by the Nrg-1 intracellular domain. J. Cell Biol. 161, 1133–1141. https://doi.org/10.1083/jcb.200212085.

Baron, A.T., et al., 2009. Clinical implementation of soluble EGFR (sEGFR) as a theragnostic serum biomarker of breast, lung and ovarian cancer. IDrugs 12, 302–308.

Brooks, B.R., et al., World Federation of Neurology Research Group on Motor Neuron Diseases, 2000. El Escorial revisited: revised criteria for the diagnosis of amyotrophic lateral sclerosis. Amyotroph. Lateral Scler. Other Motor Neuron Disord. 1, 293–299.

Carpenter, G., 2003. ErbB-4: mechanism of action and biology. Exp. Cell Res. 284, 66–77.

Chattopadhyay, S., Shubayev, V.I., 2009. MMP-9 controls Schwann cell proliferation and phenotypic remodeling via IGF-1 and ErbB receptor-mediated activation of MEK/ERK pathway. Glia 57, 1316–1325. https://doi.org/10.1002/glia.20851.

Chen, Y.-J., et al., 2010. ErbB4 in parvalbumin-positive interneurons is critical for neuregulin 1 regulation of long-term potentiation. Proc. Natl. Acad. Sci. U. S. A. 107, 21818–21823. https://doi.org/10.1073/pnas.1010669107.

Cheng, Q.-C., et al., 2003. Ectodomain cleavage of ErbB-4: characterization of the cleavage site and m80 fragment. J. Biol. Chem. 278, 38421–38427. https://doi.org/10.1074/jbc.M302111200.

Chong, V.Z., et al., 2008. Elevated neuregulin-1 and ErbB4 protein in the prefrontal cortex of schizophrenic patients. Schizophr. Res. 100, 270–280. https://doi.org/10.1016/j.schres.2007.12.474.

De Strooper, B., et al., 1999. A presenilin-1-dependent gamma-secretase-like protease mediates release of Notch intracellular domain. Nature 398, 518–522. https://doi.org/10.1038/19083.

Dols-Icardo, O., et al., 2018. Analysis of known amyotrophic lateral sclerosis and frontotemporal dementia genes reveals a substantial genetic burden in patients manifesting both diseases not carrying the C9orf72 expansion mutation. J. Neurol. Neurosurg. Psychiatry 89, 162–168. https://doi.org/10.1136/jnnp-2017-316820.

Falls, D.L., 2003. Neuregulins: functions, forms, and signaling strategies. Exp. Cell Res. 284, 14–30.

Gambarotta, G., et al., 2004. ErbB4 expression in neural progenitor cells (ST14A) is necessary to mediate neuregulin-1beta1-induced migration. J. Biol. Chem. 279, 48808–48816. https://doi.org/10.1074/jbc.M408374200.

Gambarotta, G., et al., 2015. Local delivery of the Neuregulin1 receptor ecto-domain (ecto-ErbB4) has a positive effect on regenerated nerve fiber maturation. Gene Ther. 22, 901–907. https://doi.org/10.1038/gt.2015.46.

Geng, F., et al., 2016. Neuregulin 1-ErbB4 signaling in the bed nucleus of the stria terminalis regulates anxiety-like behavior. Neuroscience 329, 182–192. https://doi.org/10.1016/j.neuroscience.2016.05.018.

Goth, C.K., et al., 2015. A systematic study of modulation of ADAM-mediated ectodomain shedding by site-specific O-glycosylation. Proc. Natl. Acad. Sci. U. S. A. 112, 14623–14628. https://doi.org/10.1073/pnas.1511175112.

Hansson, K.T., et al., 2017. Expanding the cerebrospinal fluid endopeptidome. Proteomics 17, 1600384. https://doi.org/10.1002/pmic.201600384.

Hollmén, M., et al., 2009. Suppression of breast cancer cell growth by a monoclonal antibody targeting cleavable ErbB4 isoforms. Oncogene 28, 1309–1319. https://doi.org/10.1038/onc.2008.481.

Hollmén, M., et al., 2012. Proteolytic processing of ErbB4 in breast cancer. PLoS One 7, e39413. https://doi.org/10.1371/journal.pone.0039413.

Homs, J., et al., 2014. Intrathecal administration of IGF-I by AAVrh10 improves sensory and motor deficits in a mouse model of diabetic neuropathy. Mol. Ther. Methods Clin. Dev. 1, 7. https://doi.org/10.1038/mtm.2013.7.

Illán-Gala, I., et al., 2018. CSF sAPPβ, YKL-40, and NfL along the ALS-FTD spectrum. Neurology 91, e1619–e1628.

Junttila, T.T., et al., 2000. Erbb4 and its isoforms: selective regulation of growth factor responses by naturally occurring receptor variants. Trends Cardiovasc. Med. 10, 304–310.

Lasiene, J., et al., 2016. Neuregulin 1 confers neuroprotection in SOD1-linked amyotrophic lateral sclerosis mice via restoration of C-boutons of spinal motor neurons. Acta Neuropathol. Commun. 4, 15. https://doi.org/10.1186/s40478-016-0286-7.

Lee, H.-J., et al., 2002. Presenilin-dependent gamma-secretase-like intramembrane cleavage of ErbB4. J. Biol. Chem. 277, 6318–6323. https://doi.org/10.1074/jbc.M110371200.

Lichtenthaler, S.F., et al., 2018. Proteolytic ectodomain shedding of membrane proteins in mammals-hardware, concepts, and recent developments. EMBO J. 37 (pii: e99456).

Lillo, P., Hodges, J.R., 2010. Cognition and behaviour in motor neurone disease. Curr. Opin. Neurol. 23, 638–642. https://doi.org/10.1097/WCO.0b013e3283400b41.

Loeb, J.E., et al., 1999. Enhanced expression of transgenes from adeno-associated virus vectors with the woodchuck hepatitis virus posttranscriptional regulatory element: implications for gene therapy. Hum. Gene Ther. 10, 2295–2305. https://doi.org/10.1089/10430349950016942.

Lomen-Hoerth, C., et al., 2003. Are amyotrophic lateral sclerosis patients cognitively normal? Neurology 60, 1094–1097.

Lynch, C.C., et al., 2007. Matrix metalloproteinase 7 mediates mammary epithelial cell tumorigenesis through the ErbB4 receptor. Cancer Res. 67, 6760–6767. https://doi.org/10.1158/0008-5472.CAN-07-0026.

Ma, Z., Li, Q., et al., 2009. Targeting human epidermal growth factor receptor signaling with the neuregulin's heparin-binding domain. J. Biol. Chem. 284, 32108–32115. https://doi.org/10.1074/jbc.M109.032714.

Määttä, J.A., et al., 2006. Proteolytic cleavage and phosphorylation of a tumor-associated ErbB4 isoform promote ligand-independent survival and cancer cell growth. Mol. Biol. Cell 17, 67–79. https://doi.org/10.1091/mbc.e05-05-0402.

Mancuso, R., et al., 2011. Evolution of gait abnormalities in SOD1(G93A) transgenic mice. Brain Res. 1406, 65–73. https://doi.org/10.1016/j.brainres.2011.06.033.

Mancuso, R., et al., 2016. Neuregulin-1 promotes functional improvement by enhancing collateral sprouting in SOD1(G93A) ALS mice and after partial muscle denervation. Neurobiol. Dis. 95, 168–178. https://doi.org/10.1016/j.nbd.2016.07.023.

Ni, C.Y., et al., 2001. Gamma -Secretase cleavage and nuclear localization of ErbB-4 receptor tyrosine kinase. Science 294, 2179–2181. https://doi.org/10.1126/science.1065412.

Pascal, D., et al., 2014. Characterization of glial cell models and in vitro manipulation of the neuregulin1/ErbB system. Biomed. Res. Int. 2014, 310215. https://doi.org/10.1155/2014/310215.

Phukan, J., et al., 2012. The syndrome of cognitive impairment in amyotrophic lateral sclerosis: a population-based study. J. Neurol. Neurosurg. Psychiatry 83, 102–108. https://doi.org/10.1136/jnnp-2011-300188.

Piedra, J., et al., 2015. Development of a rapid, robust, and universal picogreen-based method to titer adeno-associated vectors. Hum. Gene Ther. Methods 26, 35–42. https://doi.org/10.1089/hgtb.2014.120.

Plowman, G.D., et al., 1993. Ligand-specific activation of HER4/p180erbB4, a fourth member of the epidermal growth factor receptor family. Proc. Natl. Acad. Sci. U. S. A. 90, 1746–1750.

Portelius, E., et al., 2010. Identification of novel N-terminal fragments of amyloid precursor protein in cerebrospinal fluid. Exp. Neurol. 223, 351–358. https://doi.org/10.1016/j.expneurol.2009.06.011.

Ringholz, G.M., et al., 2005. Prevalence and patterns of cognitive impairment in sporadic ALS. Neurology 65, 586–590. https://doi.org/10.1212/01.wnl.0000172911.39167.b6.

Rio, C., et al., 2000. Tumor necrosis factor-alpha-converting enzyme is required for cleavage of erbB4/HER4. J. Biol. Chem. 275, 10379–10387.

Ripps, M.E., et al., 1995. Transgenic mice expressing an altered murine superoxide dismutase gene provide an animal model of amyotrophic lateral sclerosis. Proc. Natl. Acad. Sci. U. S. A. 92, 689–693.

Roskoski, R., 2014. The ErbB/HER family of protein-tyrosine kinases and cancer. Pharmacol. Res. 79, 34–74. https://doi.org/10.1016/j.phrs.2013.11.002.

Sanderson, M.P., et al., 2006. Control of ErbB signaling through metalloprotease mediated ectodomain shedding of EGF-like factors. Growth Factors 24, 121–136. https://doi.org/10.1080/08977190600634373.

Sardi, S.P., et al., 2006. Presenilin-dependent ErbB4 nuclear signaling regulates the timing of astrogenesis in the developing brain. Cell 127, 185–197. https://doi.org/10.1016/j.cell.2006.07.037.

Scarfò, I., et al., 2016. Identification of a new subclass of ALK-negative ALCL expressing aberrant levels of ERBB4 transcripts. Blood 127, 221–232. https://doi.org/10.1182/blood-2014-12-614503.

Schwenk, B.M., et al., 2016. TDP-43 loss of function inhibits endosomal trafficking and alters trophic signaling in neurons. EMBO J. 35, 2350–2370.

Song, F., et al., 2012. Aberrant neuregulin 1 signaling in amyotrophic lateral sclerosis. J. Neuropathol. Exp. Neurol. 71, 104–115.

Strong, M.J., et al., 2017. Amyotrophic lateral sclerosis - frontotemporal spectrum disorder (ALS-FTSD): revised diagnostic criteria. Amyotroph. Lateral Scler. Frontotemporal Degener. 18, 153–174. https://doi.org/10.1080/21678421.2016.1267768.

Takahashi, Y., et al., 2013. ERBB4 mutations that disrupt the neuregulin-ErbB4 pathway cause amyotrophic lateral sclerosis type 19. Am. J. Hum. Genet. 93, 900–905. https://doi.org/10.1016/j.ajhg.2013.09.008.

Thompson, M., et al., 2007. Widespread expression of ErbB2, ErbB3 and ErbB4 in non-human primate brain. Brain Res. 1139, 95–109. https://doi.org/10.1016/j.brainres.2006.11.047.

Thomson, R.B., et al., 2016. N-glycosylation critically regulates function of oxalate transporter SLC26A6. Am. J. Physiol. Cell Physiol. 311, C866–C873. https://doi.org/10.1152/ajpcell.00171.2016.

Tian, J., et al., 2017. Down-regulation of neuregulin1/ErbB4 signaling in the hippocampus is critical for learning and memory. Mol. Neurobiol. 54, 3976–3987. https://doi.org/10.1007/s12035-016-9956-5.

Tidcombe, H., et al., 2003. Neural and mammary gland defects in ErbB4 knockout mice genetically rescued from embryonic lethality. Proc. Natl. Acad. Sci. U. S. A. 100, 8281–8286. https://doi.org/10.1073/pnas.1436402100.

Tvorogov, D., et al., 2009. Somatic mutations of ErbB4: selective loss-of-function phenotype affecting signal transduction pathways in cancer. J. Biol. Chem. 27, 5582–5591.

Vecchi, M., Carpenter, G., 1997. Constitutive proteolysis of the ErbB-4 receptor tyrosine kinase by a unique, sequential mechanism. J. Cell Biol. 139, 995–1003.

Vecchi, M., et al., 1996. Selective cleavage of the heregulin receptor ErbB-4 by protein kinase C activation. J. Biol. Chem. 271, 18989–18995.

Wegorzewska, I., et al., 2009. TDP-43 mutant transgenic mice develop features of ALS and frontotemporal lobar degeneration. Proc. Natl. Acad. Sci. U. S. A. 106, 18809–18814.

Wen, L., et al., 2010. Neuregulin 1 regulates pyramidal neuron activity via ErbB4 in parvalbumin-positive interneurons. Proc. Natl. Acad. Sci. U. S. A. 107, 1211–1216. https://doi.org/10.1073/pnas.0910302107.

Woo, R.-S., et al., 2007. Neuregulin-1 enhances depolarization-induced GABA release. Neuron 54, 599–610. https://doi.org/10.1016/j.neuron.2007.04.009.

Xiao, X., et al., 1998. Production of high-titer recombinant adeno-associated virus vectors in the absence of helper adenovirus. J. Virol. 72, 2224–2232.

Yu, W.-H., et al., 2002. CD44 anchors the assembly of matrilysin/MMP-7 with heparin-binding epidermal growth factor precursor and ErbB4 and regulates female reproductive organ remodeling. Genes Dev. 16, 307–323. https://doi.org/10.1101/gad.925702.

Zeng, F., et al., 2007. ErbB4 isoforms selectively regulate growth factor induced Madin-Darby canine kidney cell tubulogenesis. Mol. Biol. Cell 18, 4446–4456. https://doi.org/10.1091/mbc.e07-03-0223.

Zolotukhin, S., et al., 1999. Recombinant adeno-associated virus purification using novel methods improves infectious titer and yield. Gene Ther. 6, 973–985. https://doi.org/10.1038/sj.gt.3300938.